*Journal of Modern Optics*, 2014
Vol. 61, No. 13, 1069–1076, http://dx.doi.org/10.1080/09500340.2014.920056

Taylor & Francis
Taylor & Francis Group

# Highly confined photonic nanojet from elliptical particles

T. Jalali[a]* and D. Erni[b]

[a] *Physics Department, Persian Gulf University, Bushehr, Iran;* [b] *General and Theoretical Electrical Engineering (ATE), Faculty of Engineering, University of Duisburg-Essen, and CENIDE – Center of Nanointegration Duisburg-Essen, Duisburg, Germany*

(*Received 1 February 2014; accepted 14 April 2014*)

Elliptically shaped particles with different size and refractive indices have been studied under plane wave illumination using simulation tools such as 2D-FDTD, 2D-MMP, and 3D-MMP. Owing to careful manipulation, the power distribution in the vicinity of the particles opposite boundary resulted in a tightly focused photonic nanojet. Their waists are significantly smaller than the diffraction limit while propagating over several optical wavelengths without significant divergence. In this paper, we report on the manipulation of the particles elliptical shapes and the underlying refractive indices with respect to a maximally confined power distribution in the resulting nanojet which has been parameterized according to both, the beam waist and the beam divergence. The result that elliptical particles (i.e. oblate spheroids) turned out to be superior to spherical ones was underpinned within a highly accurate and fast 3D-MMP simulation using ring multipoles.

**Keywords:** FDTD method; MMP method; photonic nanojet; scattering

## 1. Introduction

The emergence of photonic nanojets that appear on the shadow-side of illuminated cylindrical particles has been recently studied in detail [1–9], where the particle's diameter is considered longer than the wavelength of the illuminating plane wave. The emergent nanojet extends to more than $2\lambda$ in propagation direction with a beam width well below the diffraction limit of $\lambda/2$. Here, the associated mean field of the particle surface becomes rather radiative than evanescent [5]. The nanojet yields optical intensities that are orders of magnitude larger than the one of illuminating plane wave. The possibility of undercutting the diffraction limit [3] can be useful for various applications such as scanning near-field optical microscopy (SNOM), high-resolution lithography, advanced optical (and magnetic) data storage schemes, immersion lens microscopy, and for the fluorescence imaging of living cells [5]. This would be also as well suited for ultramicroscopy technique using visible light for detecting and imaging nanoparticles such as proteins, single molecules; and monitoring molecular synthesis importance in many areas of biology, chemistry, and material sciences. Because of emergent whispering gallery mode resonances with high quality factors, these micro-spheres could be one choice for employing in tight-binding photonic devices such as coupled resonator optical waveguides [9,10,12–16]. The presence of such resonances have also turned out to be advantageous for nanoparticle sensing and manipulation [8] relying on photonic nanojets. Recently, the ultra-elongated photonic nanojets super-enhancement generated at the shadow side of multilayered micro-ellipses has been discussed in detail in Ref. [11]. The intensity strongly depends on the thickness of the individual layers. This multi-layered shell structure is useful to control the beam intensity and elongation. However, the cost for a potential elongation within this specific shell topology is the widening and a decreased peak intensity of the photonic nanojet [11].

In this paper, we report on the manipulation of various dielectric elliptical particle shapes (oblate and prolate) with respect to the focal properties of the resulting nanojet, which has been parameterized according to the beam waist and the beam divergence. The simulations have been performed using a 2D finite-difference time-domain (FDTD) scheme [17] (with a tailored material dispersion model and accurate boundary averaging features), whereas 2D and 3D reference simulations are carried out with the semi-analytical (and therefore highly accurate) multiple multipole (MMP) method [18]. Depending on the refractive index, the focal point (defined here as the point on the optical axis where the intensity yields its maximum value) can be located inside or outside the sphere or ellipse. Having a focal point properly positioned on the particles surface an interesting phenomenon occurs, providing a maximal confinement of the focal volume [13]. Elliptical particles with different

*Corresponding author. Email: jalali@pgu.ac.ir

refractive indices have been extensively studied, rendering elliptical particles as a promising candidate for highly directed 3D nanojets. Finding the appropriate refractive index of the particle will be part of a comprehensive scenario as described here. Elliptical particles may provide nanojets of a superior quality that are potentially suited for a more detailed characterization of the exposed nanostructures.

The remainder of the paper is organized as following. In Section 2, different computational schemes such as 2D-FDTD, 2D-MMP, and 3D-MMP method to deal even with distinctly resonant scattering problems are described. The numerical size manipulation scenarios are presented in Section 3 while comparing first the beam parameters of the nanojets emerging from spherical respective elliptical nanoparticles. The elliptical nanoparticles of different sizes and refractive indices are then manipulated to provide best confined nanojets, where a numerically reliable confirmation of the performance is achieved within a 3D-MMP analysis that relies on both complex origin multipoles and ring multipoles. Concluding remarks and a brief outlook are given in the last Section 4.

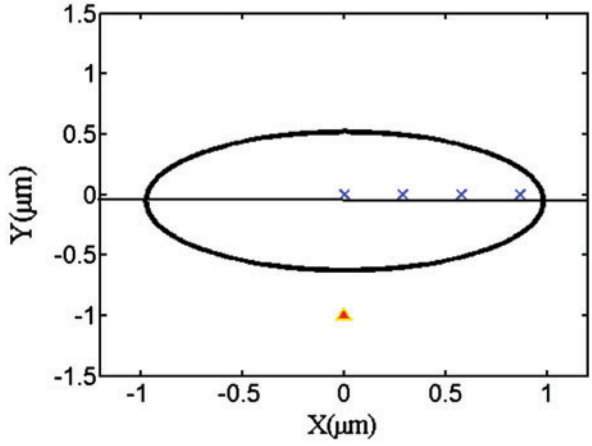


Figure 1. Elliptical boundary with four 2D multipoles located in the center, in the focal point and in between on the major axis. The triangle indicates the plane wave excitation from below. Because of the symmetry, only the right half of the computational domain is modeled. (The colour version of this figure is included in the online version of the journal.)

## 2. Simulation of elliptical nano-particles

In the realm of photonic nanojets, several numerical simulation scenarios have been reported mostly relying on dielectric microspheres [2,3]. In the following, a detailed discussion on the numerical methods is provided together with a detailed inspection of the photonic nanojet, in order to validate the unique combination of a small waist and a little beam divergence. This helps to find the near-field patterns that provide the proper optical spot size.

### *2.1. 2D-FDTD simulation*

The FDTD method has shown promise in the calculation of the scattering by realistic particles because of its ability to model complex surfaces together with detailed internal structures [10]. By using the high-resolution FDTD option in the MaX-1 MMP software [19], we could simulate the nanojet of a plane-wave-illuminated dielectric micro-ellipse, as it is shown in Figure 1. The 2D transverse magnetic (TM) case has been considered here. Convolutional perfectly matched layers (CPMLs) are used as the absorbing boundaries, where the CPML is implemented as a recursive convolution based on the time-dependent form of the stretched coordinate formulation. The code includes many different types of excitations, such as pulsed and single frequency plane wave source, Gaussian wave sources, and waveguide mode sources, and allows for an accurate treatment of material boundaries within the Yee cell [21].

### *2.2. 2D-MMP simulation*

The Multiple Multipole Program (MMP) [18,19] is a semi-analytic boundary method working in the frequency domain that may provide highly accurate results. Usually, a Generalized Point Matching (GPM) technique is applied. GPM minimizes the weighted residual associated to the boundary conditions in a set of matching points that are distributed along the boundaries between homogeneous domains. GPM usually leads to an overdetermined system of equations that is solved directly using QR decomposition. It has been shown that this method is numerically more accurate than the well-known Galerkin method that leads to symmetric square matrix systems and that is frequently used in Method of Moments (MoM) [20] codes.

In order to achieve maximum accuracy, it is important that the boundaries are not approximated by polygons, where the latter are frequently used in MoM as well in Boundary Elements Method (BEM) [21] codes. The MaX-1 code [19] that contains the latest implementation of MMP allows the user to define (i) an analytic formula (ii) analytic formulae along a so-called C-polygon, i.e. a polygon with circles inserted in the proper corner regions in such a way that the tangential direction remains continuous everywhere. Note that each corner of a C-polygon is defined by three numbers $x$, $y$, and $r$, whereas a corner of a usual polygon is only defined by the Cartesian coordinates $x$, $y$. The first derivative of the boundary curve is discontinuous in all corner points of a polygon whereas it remains continuous for the C-polygon. This is highly important because the convergence of any boundary method is the faster the higher order derivatives are held continuous. To define an ellipse in MaX-1, one can start with the definition of a circle with center $(x_o, y_o)$ and radius $r_o$, i.e. a C-polygon with a single corner $(x_o, y_o, r_o)$. This is nothing else than a parametric representation of a circle in polar coordinates with orig

$(x_o, y_o) : r(\pi) = r(0) = const$. For the ellipse, one can replace the constant $r_o$ by the formula

$$r_0^2 = 2\left(\frac{b^2}{a}\right)\varphi - \left(1 - \frac{c}{a}\right)\varphi^2 \quad (1)$$

where the parameters $a$ and $b$ are the $x$ and $y$ radii, respectively, and $c^2 = a^2 - b^2$. It should be noted that MaX-1 approximates the resulting curve with cubic splines. Therefore, it introduces some minor errors but these deviations are much smaller than those introduced by the standard polygon approximations (when the number of spline points is the same as the number of polygon points) because the second-order derivatives are still continuous.

In the Method of Auxiliary Sources (MAS) [22] – that is closely related to MMP – the scattered field outside an elliptic body is approximated by a set of monopole sources, i.e. zero-order multipoles, located on an auxiliary line along the elliptic boundary. From conformal mapping, one finds that cofocal ellipses define optimal auxiliary lines. The further away from the boundary the auxiliary line is, the more accurate the results become – at the cost of an increasingly high condition number of the system matrix. In the extreme case, one obtains a straight line between the foci of the ellipse as an optimal auxiliary line. Therefore, a multipole distribution with a multipole in each focal point and a few multipoles in between provide highly accurate results. Akkermans [23] demonstrated that even more efficient simulations were obtained when the locations of the origins of the multipoles $(x_i, y_i)$ were located in the complex plane, i.e. when $x_i$ and $y_i$ are complex numbers. Similarly, one may proceed for modeling the field inside the elliptical particle and approximate it by a set of complex origin Bessel expansions.

It is important to know that there is a high degree of freedom in setting auxiliary sources (monopoles) along some auxiliary lines [24]. For standard multipoles, one can select the orders in addition to the locations and the complex origins further increase the degree of freedom. For getting benefits out of this high degree of freedom, one must appropriately set the complex origins and multipole orders. Finding an optimal set of complex origin multipoles for a given configuration is time consuming and requires a sophisticated analysis but finding a sub-optimal but efficient set is rather easy because MaX-1 already provides applicable multipole setting routines.

Comparisons of various sub-optimal sets of multipoles give useful information for the validation of the results. Furthermore, MMP offers the possibility to compute the matching errors along the boundaries. Finally, because of the fast convergence of MMP solutions, one may obtain highly accurate results even in the close near field, i.e. where the nanojets are observed. Therefore, MMP may provide reference solutions as long as pure analytic solutions are missing.

### *2.3. 3D-MMP simulation*

For generating general 3D objects in MaX-1, the procedure is similar to 2D, i.e. only the boundaries are needed to be specified and the discretization of the boundaries should be performed as accurately as possible, namely without approximations by triangular flat elements as used in BEM. For axisymmetric 3D problems, one may take advantage of a symmetry-adapted formalism where only one section of the boundary is defined followed by a symmetry decomposition of the multipole expansions. The present version of MaX-1 [19] does not include a MMP version for axisymmetric problems. Therefore, we have used a general 3D-MMP solver as outlined in [18]. This contains the possibility to create 3D boundaries by rotating 2D boundaries around an axis. Therefore, one can take advantage of the 2D models mentioned in the previous section for modeling, e.g. 3D axisymmetric particles. The symmetry decomposition of the multipole expansions is more demanding, except when the excitation is a plane wave, a Gaussian beam, or a multipole field that propagates along the axis.

In this case, the excitation has the angular dependence $\cos(n\varphi)$ or $\sin(n\varphi)$, where $n = 1$ for both, the plane wave and the Gaussian beam. Obviously, the scattered field yields the same angular dependence $\cos(n\varphi)$ or $\sin(n\varphi)$ with the same value $n$ as the excitation. Hence, a symmetry-adapted set of complex origin multipoles is easily defined. In case of real origin multipoles, the symmetry-adaptation is straightforward for multipoles with origins on the optical axis. One then simply has to select the orientation of the multipole in such a way that its axis coincides with the symmetry axis. For prolate spheroids (ellipse rotated around its major axis), it is sufficient to place multipoles only on the symmetry axis. Therefore, symmetry adaptation becomes very feasible. For oblate spheroids (ellipse rotated around its minor axis), off-axis multipoles are required for obtaining accurate results. The symmetry adaptation then leads to so-called ring multipoles that are also contained in MaX-1. For complex origin multipoles, the situation is easier because one may place the real part of all complex origins on the symmetry axis for both prolate and oblate spheroids. Furthermore, the imaginary component of the origin in all directions perpendicular to the symmetry axis must be zero, i.e. only one imaginary component of the origin needs to be specified provided that the multipole axis coincides with the symmetry axis. Incidentally, ring multipoles and complex origin multipoles are closely related. MaX-1 provides routines for converting 2D off-axis multipoles in 3D ring multipoles and 3D ring multipoles into complex origin multipoles. For the results shown in the next section, both ring multipoles and complex origin multipoles were applied.

## 3. Particle shapes for proper nanojet emission

Recent simulations have revealed that not only an infinite dielectric cylinder but also a dielectric sphere with a

diameter of around 10λ is capable to focus light beyond the diffraction limit [1,3,8]. Depending on the refractive index, the focal point can lie either inside or outside of the micro-ellipse. Along the propagation distance, the full width half maximum (FWHM) of the emerging beam remains always below the wavelength limit while reaching very high light intensities. We have analyzed the focal properties of the emerging nanojets within two different scenarios, by using, first, 2D-FDTD [25] respective 2D-MMP, and second, 3D-MMP. The FDTD method was used exclusively for 2D models, but not for 3D, since we have to apply a very fine mesh ($dx = 5\,\text{nm}$) to approximate both the nanojet and the underlying micro-sphere or micro-ellipse. In 3D, the computational domain becomes untractable even for a high-end PCs not to mention the large computation time imposed by the Courant-Freidrich-Levy (CFL) criterion. A possible loophole may be provided in the framework of an equivalent-circuit-(EC)-FDTD engine with symmetry adapted grids and sub-gridding capabilities [26].

### 3.1. 2D nanojet manipulation scenarios

We proceeded our study while investigating the internal field and the external near fields of a series of homogeneous, isotropic, dielectric micro-ellipses in full details. The resulting nanojet of microellipse is compared to the resulting nanojet of micro-sphere. Therefore, we kept $R_x = r_{sphere} = 5\,\mu\text{m}$, while in order to achieve a comparable nanojet in the immediate vicinity of the ellipse's shadowside boundary, we need to alter the refractive index accordingly. The dielectric micro-cylinder is illuminated by a plane wave with unit amplitude and an operating wavelength of $\lambda = 500\,\text{nm}$. The structure shown in of Figure 2 is a circular cylinder with a radius of $5\,\mu\text{m}$ with a refractive index of $n = 1.54$ surrounded by air, whereas Figure 2(*b*) displays a cylinder with elliptical cross-section ($n = 1.4$, surrounded by air) having $R_y = 0.9R_x = 4.5\,\mu\text{m}$ and $R_x = 5\,\mu\text{m}$ as the semi-minor respective semi-major axis. Hence, circular and elliptical particles with different refractive indices have been extensively analyzed, rendering elliptical particles as the most promising candidates for highly directed nanojets. Figure 2 illustrates the time-averaged poynting field distribution. The field peak emerges at the shadow side of the 2D micro-cylinder and the extends as a nanojet with little beam divergence into the surrounding medium. By increasing surrounding refractive index, the nanojet moves from the inside to the outside of the micro-cylinder while crossing the boundary in the propagating direction. At the boundary, a maximum beam confinement may be expected due to the presence of strongly confined evanescent fields.

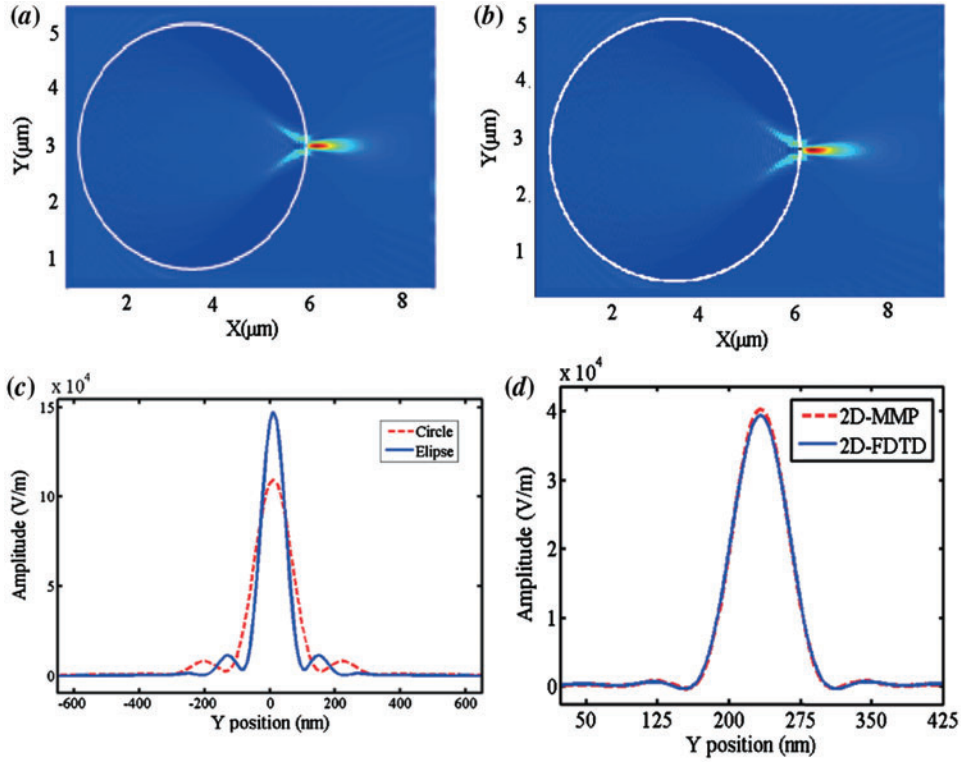


Figure 2. 2D-FDTD analysis of the time-averaged Poynting field for particles with: (*a*) circular shape and $R = 5\,\mu\text{m}$, $n = 1.54$; and (*b*) elliptical shape with $R_y = 0.9$, $R_x = 4.5\,\mu\text{m}$, $n = 1.4$ yielding (*c*) a beam waists of $W_{FWHM} = 240$ and 200 nm for the circular and the elliptical particle, respectively, (*d*) shows a numerical comparison for a circular particle with $R = 1\mu\text{m}$, $n = 1.59$ yielding a beam waist of $W_{FWHM} = 141$ nm. (The colour version of this figure is included in the online version of the journal.)

The FWHM waists of circular and elliptical micro-cylinders are 240 and 200 nm, and the lengths of nanojets expand over 900 and 1050 nm, and the intensity is enhanced by a factor of 105 compared to the illuminating plane wave. A comparison between the circular and the elliptical particle is given in Figure 2(*c*), renderig the elliptical particle superior with respect to the maximal beam intensity and the narrow beam waist.

Particles of elliptical shape pose an additional challenge when tracking down proper nanojets with respect to the associated refractive indices and particle sizes. The oblate ellipse is manipulated by altering the major axis $R_y$. Then for obtaining the optimal nanojet, the refractive index is varied in such a way that the focal point gets located on the particle surface. The excitation is given by a plane wave that emerges from the left boundary of the computational domain, having an operating wavelength $\lambda = 500\,\text{nm}$. CFL-stability is ensured while choosing a time step according to $0.95/c_0(\triangle x^2 + \triangle y^2)^{0.5}$, where $c_0$ is the speed of light. Discretization uses a Cartesian grid with $dx = dy = 5\,\text{nm}$ and the number of CPML layers is 24 in order to terminate the outer boundary of the computational domain. Figure 2(*d*) shows a good agreement between 2D-MMP and 2D-FDTD for a circular micro-cylinder with $R = 1\,\mu\text{m}$, $n = 1.59$. The beam waist size is nearly 141 nm which agrees well with Ref [5] (and here in particular Figure 4(*b*) and corresponding result) [5].

Figure 3(*a*)–(*d*) visualize the internal field and the external near field of each elliptical micro-cylinder for four different sets of semi-minor axes $R_x$, semi-major axes $R_y$, and the particle refractive index $n$, namely: ($R_x = 6\,\mu\text{m}/R_y = 7.8\,\mu\text{m}/n = 2.1$), ($R_x = 6\,\mu\text{m}/R_y = 9\,\mu\text{m}$, $n = 2.45$), ($R_x = 6\,\mu\text{m}/R_y = 12.0\,\mu\text{m}$ / $n = 2.9$), and ($R_x = 6\,\mu\text{m}/R_y = 13.2\,\mu\text{m}$ / $n = 3.0$), respectively. With increasing length of the semi-major axis $R_y$, the focal point (in particular the point of maximum field intensity) shifts from the inside to the outside while crossing the elliptical boundary. Therefore, we manipulated the nanojet while tracking down the refractive index that locates the focal point on the proper boundary. A quantitative account of the beam waist with respect to the variation of $R_y$ and $n$ is depicted in Figure 4. It is worth mentioning that the associated maximal intensity

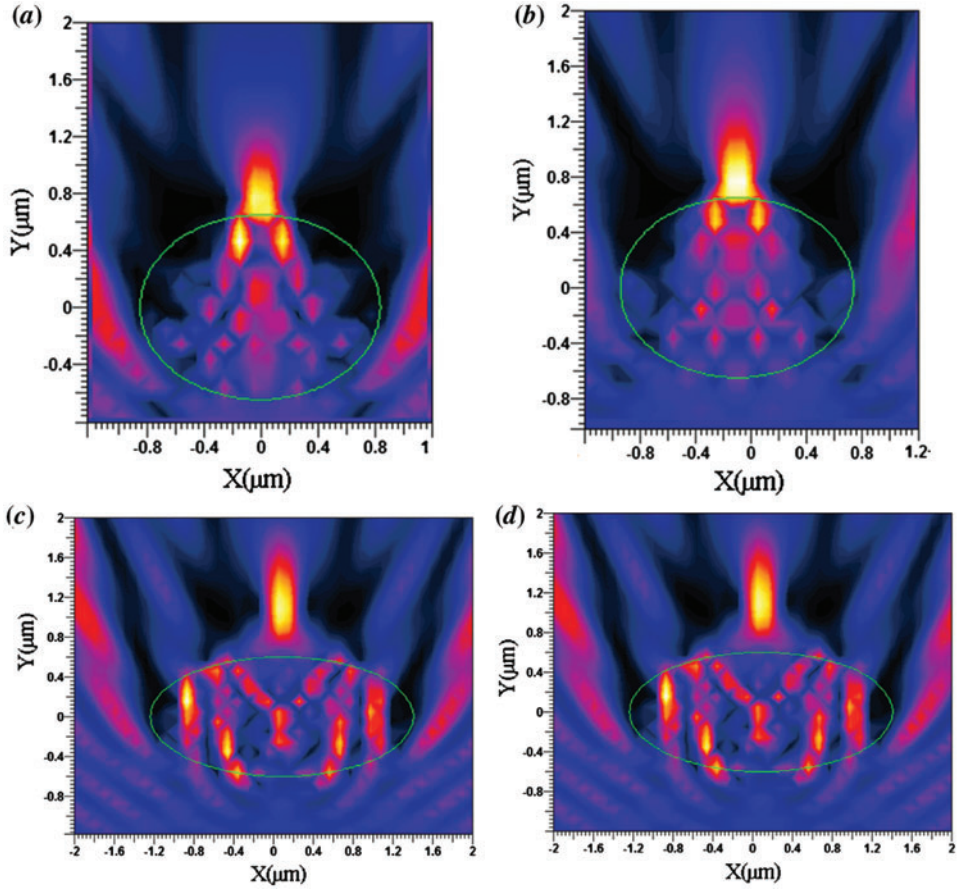


Figure 3. 2D-MMP simulation of the time-averaged Poynting field for elliptical particles with $R_x = 6\,\mu\text{m}$, and (*a*) $R_y = 7.8\,\mu\text{m}$, $n = 2.1$; (*b*) $R_y = 9\,\mu\text{m}$, $n = 2.45$; (*c*) $R_y = 12.0\,\mu\text{m}$, $n = 2.9$; (*d*) $R_y = 13.2\,\mu\text{m}$, $n = 3.0$. (The colour version of this figure is included in the online version of the journal.)

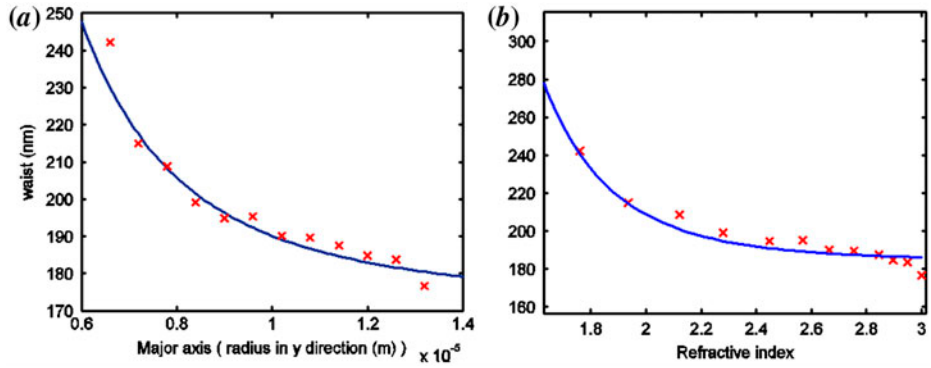


Figure 4. Evolution of the beam waist for an elliptical particle having a constant (*a*) $R_x = 6\,\mu\text{m}$, $n$ =2.1 and (*b*) $R_x = 6\,\mu\text{m}$, $R_y = 7.8\,\mu\text{m}$ while undergoing the indicated variations of either $R_y$ or $n$. (The colour version of this figure is included in the online version of the journal.)

of the emergent nanojet is somehow inversely related to the occurring beam waist. Strong focusing with a beam waist of only $W_{FWHM} = 114\,\text{nm}$ was achieved within the 2D simulation scenario ($R_x = 6\,\mu\text{m}$, $R_y = 13.2\,\mu\text{m}$, $n = 3$), which is well below one-half of the wavelength.

It turns out that the FWHM beam waist for the oblate ellipse is narrower (with higher beam intensity) than for the prolate one. Thus, the oblate ellipse is further studied by changing their axis sizes, the refractive index of the particle and the surrounding medium. The proper focal point remains located on the particle surface, although the surrounding refractive index is altered. Furthermore, the nanojet intensity grows with increasing refractive index and semi-major axis of the micro-cylinder Figure (4(*a*)). The relative increase of the refractive index relative to the surrounding medium and the associated intensity enhancement go along with a shortening of the photonic nanojet's longitudinal extent Figure (4(*b*)). Even though the 2D-FDTD method is easy to implement, it becomes memory intensive and time consuming for the desired accuracy. Therefore, this method is not practical for the investigation of nanojets where a very fine mesh is needed and several iterations are carried out.

### *3.2. 3D nanojet manipulation scenarios*

As it is mentioned in ref. [5], a set of isotropic and dielectric microspheres of different refractive indices which are illuminated by a plane wave has been analyzed and discussed in detail. They create a pencil-like 3D photonic nanojet that shows weak sub-diffraction within a minimized beam width. The 3D nanojet shapes turn out to be similar to their 2D versions. However, the 3D nanojets provide an even higher intensity compared to the 2D nanojets generated by corresponding dielectric cylinders [6]. The simulation domain for a proper 3D analysis that conforms to a smooth particle surface requires almost $3000 \times 3000 \times 3000$ cells yielding a cubic physical space with 7 $\mu$m side length. Such fine discretization renders the numerical analysis on a single PC barely tractable, not to mention any numerical investigation, manipulation, or optimization scenarios. Hence, spheroidal particles, which are promising structures to obtain 3D nanojets, are therefore investigated using the 3D-MMP method. In case of an oblate ellipsoid, an ellipse is rotated around its short axis to provide the intended geometry, which is then introduced into the MMP model.

Figure 5(*a*) depicts the time-averaged Poynting field of a photonic nanojet emerging from an oblate spheroid, where the latter is illuminated by a plane wave from the opposite side. The aspect ratio of the spheroid axes is 1:2 with $R_x = 6\,\mu\text{m}$, $R_y = 12\,\mu\text{m}$, and the refractive index amounts to $n = 2.9$ Figure 3(*b*). One of the parameters of the 2D model is used to compute the waist size. As it is shown in Figure 5(*b*), the nanojet yields a FWHM beam waist of about 170 nm. In Figure 5, complex origin multipoles are applied to model the beam shape of the nanojet. The main drawback of complex origin models is that there is a cut (for each complex origin multipole) that may not cross the boundary of the corresponding domain. This is only possible for simply connected domains. In Figure 5, corresponding ring multipoles are therefore used. Ring multipoles may provide better field approximations to the given geometry but require numerical integrations, which add to the simulation time and potentially cause numerical inaccuracies mainly with respect to radiation the $\varphi$ direction. The comparison between these two methods shows that the complex origin could save both, memory and simulation time, but there is – as intended – no significant difference in the resulting nanojet. Regarding the spheroid simulations, the relative matching error is 1.27% for the ring multipoles and 5.3% for the complex origin multipoles. The associated simulation time is 14 s for the ring multipoles and 5 s in the case of the complex origin multipoles. Therefore, numerical calculations using symmetry decomposition for both, complex origin and ring multipoles are very fast and highly accurate rendering MMP the method of choice for photonic nanojet simulations.

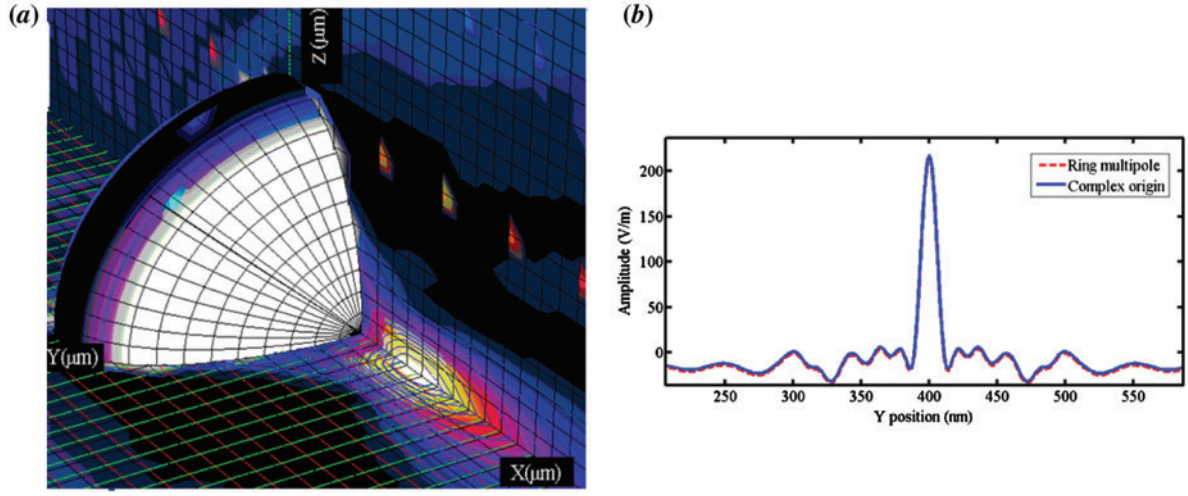


Figure 5. (*a*) 3D-MMP simulation of the time-averaged Poynting field for 3D elliptical particles. (*b*) The beam waist is $W_{FWHM} = 170\,\text{nm}$ for a ellipsoid with $R_x = 5\,\mu\text{m}$, $R_y = 2.5\,\mu\text{m}$, $n = 2.1$ using models with complex origin multipoles (solid line); ring multipoles (dashed line). (The colour version of this figure is included in the online version of the journal.)

## 4. Conclusions and outlook

In this paper, we have shown that tightly focused photonic nanojets emerges not only from spherical (and circular) dielectric particles but even though from oblate spheroids (and elliptical particles). By tuning the aspect ratio of the axes and by carefully choosing the refractive index for both, particle and surrounding medium, an manipulated nanojet is achieved with the focal point located in the proper vicinity of the surface that lies on the shadow side of the illuminated particle. With the extension of spherical particles to spheroids, an additional degree of freedom is gained that helps to design properly confined nanojets even for materials with given refractive indices. In the framework of the highly accurate and fast 3D-MMP method, we have analyzed the unique properties of emerging nanojets using ring multipoles and complex origin multipoles as highly adapted approximation basis for the nanojet field. A comparison between oblate and prolate spheroids shows that both shapes yield nearly the same beam waist, although the intensity of oblate spheroid is 1.5 times is larger in relation to the oblate shape. The beam waist gets even narrower when increasing both the major axis and the particles refractive index. Such parametrization turns out to become particularly advantageous when designing tightly confined photonic nanojets for future applications such as e.g. ultra-sensitive particle senors, optically driven pumps for microfluidics, and highly selective optical tweezers [8].

## References

[1] Itagi, A.V.; Challener, W.A. *J. Opt. Soc. Am. A* **2005,** *22,* 2847–2858.
[2] Lecher, S.; Takakura, Y.; Meyrueis, P. *Opt. Lett.* **2005,** *30,* 2641–2643.
[3] Chen, Z.; Taflove, A.; Backman, V. *Opt. Express* **2004,** *12,* 1214–1220.
[4] Betzig, E. *Opt. Lett.* **1995,** *20,* 237–239.
[5] Heifetz, A.; Kong, S.-C.; Sahakian, A.V.; Taflove, A.; Backman, V. *J. Comput. Theor. Nanosci.* **2009,** *6,* 1979–1992.
[6] Ruiz, C.M.; Simpson, J.J. *Opt. Express* **2010,** *18,* 16805–16812.
[7] Ferrand, P.; Wenger, J.; Devilez, A.; Pianta, M.; Stout, B.; Bonod, N.; Popov, E.; Rigneault, H. *Opt. Express* **2008,** *16,* 6930–6940.
[8] Cui, X.; Erni, D.; Hafner, C. *Opt. Express* **2008,** *16,* 13560–13568.
[9] Kim, M.S.; Scharf, T.; Mühlig, S.; Rockstuhl, C.; Herzig, H.P. *Opt. Express* **2011,** *19,* 10206–10220.
[10] Stefanou, N.; Modinos, A. *Phys. Rev. B* **1998,** *57,* 12127–12133.
[11] Liu, C. *PIER Lett.* **2013,** *37,* 153–165.
[12] Chen, Z.; Taflove, A.; Backman, V. *Opt. Lett.* **2006,** *31,* 389–391.
[13] Jalali, T.; Erni, D.; Hafner, Ch. *Molding the Emission of Photonic Nanojets by Different Particle Shapes* XV International Workshop on Optical Waveguide Theory and Numerical Modeling (OWTNM 2006); Varese, Italy, 2006.
[14] Jalali, T. *J. opt* **2014,** *16,* 035705 1–6.
[15] Bohren, C.F.; Huffman, D.R. *Absorption and Scattering by Small Particles*; John Wiley & Sons: New York, 1998.
[16] Asano, S.; Yamamoto, G. *Appl. Opt.* **1974,** *14,* 29–48.
[17] Taflove, A.; Hagness, S. *Computational Electrodynamics: The Finite-Difference Time-Domain Method*; Artech House: Boston, 2000.
[18] Hafner, Ch. *Post-modern Electromagnetics*; John Wiley & Sons: New York, 1999.
[19] Hafner, Ch. *MaX-1: A Computational Electromagnetics Platform Based on the Multiple Multipole (MMP) Method*. http://max-1.ethz.ch (accessed May 10, 2014).
[20] Harrington, R.F. *Field Computation by Moment Methods*; Macmillan: New York, 1968.
[21] Banerjee, P.K. *The Boundary Element Methods in Engineering*; McGraw-Hill: London, 1994.

[22] Wriedt, T. *Generalized Multipole Techniques for Electromagnetic and Light Scattering*; Elsevier: Amsterdam, 1999.
[23] Akkermans, G.P.M. *National Technical Information Service*; Springer-Verlag: Berlin, 1982.
[24] Hafner, Ch. *Phys. Status Solidi B-Basic Solid State Phys.* **2007,** *244,* 3435–3447.
[25] Jalali, T.; Jalali, D.E.; Rauscher, K.; Mohammadi, A.; Erni, D.; Hafner, Ch.; Baechtold, W.; Shoushtari, M.Z. *J. Comput. Theor. Nanosci.* **2007,** *4,* 644–648.
[26] Liebig, T.; Rennings, A.; Held, S.; Erni, D. *Int. J. Numer. Model. Special Issue Optim.* **2013,** *26,* 680–696. doi:10.1002/jnm.1875.